A small molecule nanodrug consisting of amphiphilic targeting ligand–chemotherapy drug conjugate for targeted cancer therapy

Quanbing Mou, Yuan Ma, Xinyuan Zhu, Deyue Yan

PII: S0168-3659(16)30183-3
DOI: doi: 10.1016/j.jconrel.2016.03.037
Reference: COREL 8199

To appear in: *Journal of Controlled Release*

Received date: 5 December 2015
Revised date: 1 March 2016
Accepted date: 28 March 2016

Please cite this article as: Quanbing Mou, Yuan Ma, Xinyuan Zhu, Deyue Yan, A small molecule nanodrug consisting of amphiphilic targeting ligand–chemotherapy drug conjugate for targeted cancer therapy, *Journal of Controlled Release* (2016), doi: 10.1016/j.jconrel.2016.03.037

A small molecule nanodrug consisting of amphiphilic targeting ligand-chemotherapy drug conjugate for targeted cancer therapy

Quanbing Mou[1], Yuan Ma[1], Xinyuan Zhu[*], and Deyue Yan[*]

School of Chemistry and Chemical Engineering, State Key Laboratory of Metal Matrix Composites, Shanghai Jiao Tong University, 800 Dongchuan Road, Shanghai 200240, P. R. China.

Abstract Targeted drug delivery is a broadly applicable approach for cancer therapy. However, the nanocarrier-based targeted delivery system suffers from batch-to-batch variation, quality concerns and carrier-related toxicity issues. Thus, to develop a carrier-free targeted delivery system with nanoscale characteristics is very attractive. Here, a novel targeting small molecule nanodrug self-delivery system consisting of targeting ligand and chemotherapy drug was constructed, which combined the advantages of small molecules and nano-assemblies together and showed excellent targeting ability and long blood circulation time with well-defined structure, high drug loading ratio and on-demand drug release behavior. As a proof-of-concept, lactose (Lac) and doxorubicin (DOX) were chosen as the targeting ligand and chemotherapy drug, respectively. Lac and DOX were conjugated through a pH-responsive hydrazone group. For its intrinsic amphiphilic property, Lac-DOX conjugate could self-assemble into nanoparticles in water. Both *in vitro* and *in vivo* assays indicated that Lac-DOX nanoparticles exhibited enhanced anticancer activity and weak side effects. This novel active targeting nanodrug delivery

system shows great potential in cancer therapy.

Graphical abstract

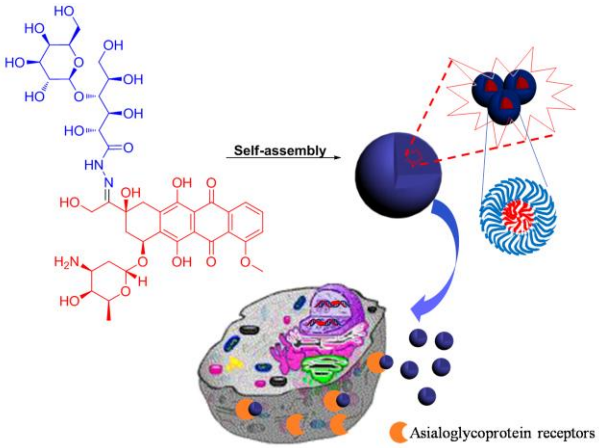

Keywords: Cancer therapy; Targeted delivery; Small molecule nanodrugs; Amphiphilic self-assembly

1. Introduction

Targeted cancer therapy has expanded tremendously in recent years. Owing to the rapid development of nanotechnology, various active targeting nanocarriers based on the modification of nanoparticles with tumor-specific molecules have been carried out. These active targeting ligands including antibodies, peptides and small molecules (e.g., folate [1], galactose [2], lactose [3]) can greatly enhance the cellular uptake of nanoparticles via receptor-mediated endocytosis. Nanocarriers used for cancer therapies such as liposomes [4-6], micelles [7-20], protein nanoparticles [21, 22], metallic nanoparticles [23-27], inorganic nanoparticles [28, 29] can passively accumulate in the tumor site through the enhanced permeability and retention (EPR) effect [30-34]. Both passive and active targeting properties endow the delivery systems with enhanced therapeutic activity. Nevertheless, the fabrication of active targeting nanocarriers is extremely complicated, including materials synthesis/assembly, ligand coupling, separation and purification, which could cause batch-to-batch variation and quality concerns [35]. Besides, the degradation, metabolism, and excretion of nanocarriers can cause significant toxicity issues [36] (e.g., mitochondrial damage, cardiovascular effects, platelet aggregation, oxidative stress, inflammation). The active targeting nano drug delivery systems with high dose use of nanocarriers do

increase the therapeutic efficiency, but nanocarriers used are potential hazards. Thus, there are only a few targeted nanodrug delivery systems in clinical trials [37]. It is an urgent demand to develop a carrier-free system with excellent targeting ability and weak side effects.

Different from the carrier-based targeted delivery systems, a carrier-free amphiphilic drug-drug conjugate (ADDC) self-delivery system from direct conjugation of hydrophobic anticancer drug with hydrophilic anticancer drug has been successfully developed in our group [38]. Inspired by the simple concept only using the amphiphilic small molecules to form micells, here we develop an active targeting small molecule nanodrug consisting of the hydrophilic targeting ligand and the hydrophobic chemotherapy drug through a bio-responsive linkage. This novel active targeting self-delivery system brings together the antigen-targeting specificity of the targeting ligand, favorable pharmacokinetics of nanomedicine and the cytotoxic potency of promising chemotherapeutic drugs. Chemotherapeutic drugs can be released in stimuli circumstance. The drug loading ratio of this active targeting self-delivery system conjugates is high, for the molecular weights of targeting ligands and anticancer drugs are in the same order of magnitude. Besides, the toxic anticancer drug moieties of the conjugates are aggregated in the core of the micelles, and surrounded by the nontoxic targeting ligands, which leads to significant reduction of the cytotoxicity to normal cells. Moreover, the active targeting self-delivery system can accumulate at the tumor site both passively and actively.

As a proof-of-concept, lactose (a small molecular weight hydrophilic hepatocyte targeting molecule, Lac) [39-41] and doxorubicin (a hydrophobic anticancer drug, DOX) are simply conjugated via a pH-responsive hydrazone group [42-45] (Lac-DOX) to form an active targeting nanodrug delivery system, as illustrated in Scheme 1. Similar to ADDC, Lac-DOX conjugate is expected to show favorable pharmacokinetics and benefits of highly potent anticancer drugs. The structure of Lac-DOX conjugate is well-defined with drug loading ratio of 61.7%. Lac-DOX conjugate self-assembles into nanoparticles for its intrinsic amphiphilic property. Self-assembled Lac-DOX nanoparticles can passively accumulate in the tumor site through EPR effect. More importantly, Lac can greatly enhance the cellular uptake of

nanoparticles via receptor-mediated endocytosis. Both passive and active targeting properties endow the delivery system with enhanced therapeutic activity.

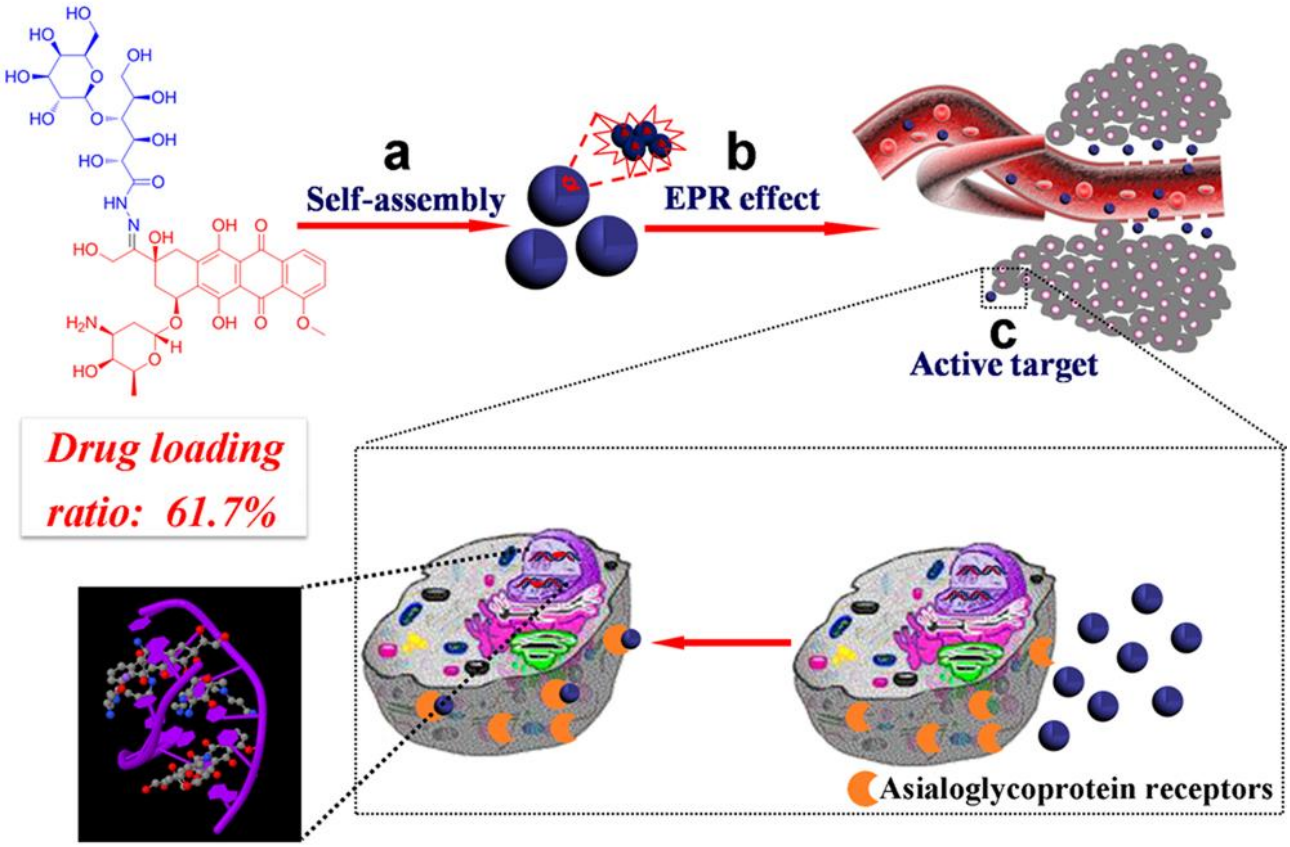

Scheme 1. Lac-DOX Nanoparticles for Passive and Active Targeting Drug Delivery. (a) Schematic illustration for the self-assembly of amphiphilic Lac-DOX. (b) Lac-DOX nanoparticles accumulated at the tumor site through both passive and active targeting mechanisms. (c) Free DOX was released from Lac-DOX nanoparticles to inhibit the proliferation of SMMC-7721 cells.

2. Materials and methods

2.1 Materials

Dimethylsulfoxide (DMSO) was dried over calcium hydride for 48 h and then distilled before use. Methanol was purchased from Hipure Chem and was high performance liquid chromatography (HPLC) grade. 3-(4,5-Dimethyl-thiazol-2-yl)-2,5-diphenyl tetrazolium bromide (MTT, Sigma), 4-O-beta-D-galactopyranosyl-D-gluconic acid (Lactobionic acid, 97%, Aladdin), hydrazine hydrate

(98%, Aladdin), and delta-gluconolactone (99%, Adamas) were used as received. Doxorubicin hydrochloride (DOX·HCl) was purchased from Beijing Huafeng United Technology Corporation.

2.2 Measurements

Nuclear magnetic resonance (NMR) spectroscopy spectra were performed on a Varian Mercury Plus 400 MHz spectrometer with deuterium oxide (D_2O) or dimethylsulfoxide-d6 (DMSO-d6) as solvents. Ultraviolet-visible absorption (UV-vis) spectra were collected on an Evolution 300 UV-vis spectrophotometer. Fourier transform infrared spectra (FT-IR) spectra were measured on a Paragon 1,000 instrument. High-resolution mass spectra (HRMS) were recorded on a Waters-ACQUITYTM UPLC & Q-TOF-MS premier. The fluorescent spectra of sample solutions were performed on a Perkin-Elmer LS-50B fluorescence spectrometer. The excitation wavelength was set at 488 nm, which was chosen according to the maximum intensity obtained in the excitation spectra. Step increment was set as 2 nm, and scan speed was set at 480 nm/min. Dynamic light scattering (DLS) measurements were performed on a Malvern Zetasizer NanoS apparatus (Malvern Instruments, Ltd.) equipped with a 4 mW laser light operating at λ = 633 nm. All samples were measured at a scattering angle of 90°. The morphology and size of nanoparticles were characterized by a Tecnai G2 Spirit Biotwin instrument at voltage of 120 kV.

2.3 Synthesis of lactobionolactone

According to the literature procedure [46] with a little modification, lactobionic acid (5.0000 g, 13.96 mmol) was dissolved in anhydrous methanol (70.0 mL) at 75 °C followed by vacuum distillation at 40 °C. The procedure was repeated until lactobionic acid was fully converted to lactobionolactone. ^{1}H NMR (400 MHz, DMSO-d_6) δ (ppm): 5.33-4.01 (br, OH), 4.34-4.13 (m, 2H, CH), 4.02-3.86 (m, 1H, CH), 3.75-3.25 (m, 10H, CH & CH_2). ^{13}C NMR (100 MHz, DMSO-d_6) δ (ppm): 173.44, 105.42, 84.19, 76.01, 73.66, 71.83, 71.63, 71.41, 70.94, 68.55, 62.64, 60.79. HRMS: (ESI) $[M-H]^-$ calcd. for $C_{12}H_{19}O_{11}$, 339.0927, found 339.0927.

2.4 Synthesis of (2R,3R,4R,5R)-2,3,5,6-tetrahydroxy-4-(((2S,3R,4S,

5R,6R)-3,4,5-trihydroxy-6-(hydroxymethyl)tetrahydro-2H-pyran-2-yl) oxy)hexanehydrazide (Lac-NHNH$_2$)

Lactobionolactone (3.0000 g, 8.82 mmol) was dissolved in anhydrous methanol (40.0 mL) at 25 ^{o}C. Hydrazine hydrate (2.2270 g, 44.10 mmol) was added dropwise to the solution of lactobionolactone via a syringe and keep at 25 ^{o}C for 1 h. The white powder was collected by a rotary evaporator (yield: 76.2%). ^{1}H NMR (400 MHz, DMSO-d_6) δ (ppm): 8.91-8.50 (s, 1H, NH), 5.23-4.03 (br, OH), 4.32-4.17 (d, J = 4.27 Hz, 1H, CH), 4.19-4.09 (d, J = 4.16 Hz, 1H, CH), 4.04-3.93 (m, 1H, CH), 3.73-3.60 (m, 2H, CH), 3.60-3.46 (m, 5H, CH & CH$_2$), 3.45-3.24 (m, 3H, CH), 3.18-3.16 (s, 2H, NH$_2$). ^{13}C NMR (100 MHz, DMSO-d_6) δ (ppm): 171.46, 104.95, 82.96, 76.15, 73.67, 72.05, 71.86, 71.56, 70.92, 68.74, 62.77, 61.15. HRMS: (ESI) $[M+H]^+$ calcd. for $C_{12}H_{20}O_{11}$, 339.0927, found 339.0927.

2.5 Synthesis of (2R,3R,4R,5R,Z)-N'-(1-(4-(((2R,4S,5S,6S)-4-amino-5-hydroxy-6-methyltetrahydro-2H-pyran-2-yl)oxy)-2,5,12-trihydroxy-7-methoxy-6,11-dioxo-1,2,3,4,6,11-hexahydrotetracen-2-yl)-2-hydroxyethylidene)-2,3,5,6-tetrahydroxy-4-(((2S,3R,4S,5R,6R)-3,4,5-trihydroxy-6-(hydroxymethyl)tetrahydro-2H-pyran-2-yl)oxy)hexanehydrazide (Lac-DOX)

Doxorubicin hydrochloride (500.0 mg, 0.86 mmol) was dissolved in anhydrous DMSO (10.0 mL). Lac-NHNH$_2$ (643.8 mg, 1.73 mmol) in 10.0 mL DMSO was added dropwise to the above solution. The resulting solution was stirred at 25 ^{o}C for 0.5 h under an atmosphere of nitrogen. After evaporation of DMSO under reduced pressure, the resulting mixture was purified by reverse phase silica gel column chromatography (gradient 2 to 20 percent acetonitrile in water) to give the title compound (250.0 mg, 32.4%). ^{1}H NMR (400 MHz, DMSO-d_6) δ (ppm): 11.68 (s, 1H, NH), 8.02 (br, 2H, NH$_2$), 7.90-7.76 (m, 2H, CH), 7.64-7.53 (d, J = 7.59 Hz, 1H, CH), 6.15-5.96 (br, OH), 5.65-4.42 (br, OH), 5.35-5.26 (m, 1H, CH), 5.08-5.01 (m, 1H, CH), 4.48 (s, 2H, CH$_2$), 4.28 (m, 1H, CH), 4.24 (m, 1H, CH), 4.16 (m, 1H, CH), 4.14 (m, 1H, CH), 3.95 (s, 3H, CH$_3$), 3.71 (m, 1H, CH), 3.70 (m, 1H, CH), 3.61 (m, 1H, CH), 3.58 (m, 1H, CH), 3.55 (m, 2H, CH$_2$), 3.46 (m, 2H, CH$_2$), 3.39 (m, 1H, CH), 3.37 (m, 1H, CH), 3.35 (m, 1H, CH), 3.30 (m, 1H, CH), 2.94 (m, 2H, CH$_2$), 2.22 (m, 2H, CH$_2$), 1.96-1.59 (m, 2H, CH$_2$), 1.26-1.12 (d, J = 1.15 Hz, 3H, CH$_3$). ^{13}C NMR (100 MHz, DMSO-d_6) δ (ppm): 186.71, 186.63, 169.06, 161.13,

158.53, 156.75, 155.13, 136.69, 136.20, 135.57, 134.95, 120.17 (overlap, 2C), 119.34, 110.82 (overlap, 2C), 105.18, 99.76, 84.01, 76.13, 73.70, 72.82, 72.10, 71.60 (overlap, 3C), 71.04, 68.57, 66.65, 66.58, 62.66, 60.93, 57.78, 57.04, 47.06, 38.33, 33.37, 28.73, 17.30. HRMS: (ESI) $[M+H]^+$ calcd. for $C_{39}H_{51}N_3O_{21}$, 898.3093, found 898.3091.

2.6 Synthesis of (2R,3R,4R,5S)-2,3,4,5,6-pentahydroxyhexane hydrazide (Glu-NHNH$_2$)

Hydrazine hydrate (7.0270 g, 140.40 mmol) was added dropwise to a solution of delta-gluconolactone (5.0000 g, 28.08 mmol) in methanol (80.0 mL) under constant stirring at 40 ^oC for 0.5 h. The white powder was collected by vacuum filtration (yield: 60.0%). ^1H NMR (400 MHz, DMSO-d_6) δ (ppm): 8.80 (s, 1H, NH), 5.26 (s, 1H, OH), 4.30-4.70 (br, 4H, OH), 4.22 (s, 2H, NH_2), 4.07-3.98 (m, 1H, CH), 3.92-3.83 (m, 1H, CH), 3.62-3.31 (m, 4H, CH & CH_2). ^{13}C NMR (100 MHz, DMSO-d_6) δ (ppm): 171.63, 73.52, 72.35, 71.89, 70.62, 63.82. HRMS: (ESI) $[M+H]^+$ calcd. for $C_6H_{15}N_2O_6$, 211.0930, found 211.0935.

2.7 Synthesis of (2R,3R,4R,5S)-N'-(1-(4-(((2R,4S,5S,6S)-4-amino-5-hydroxy-6-methyltetrahydro-2H-pyran-2-yl)oxy)-2,5,12-trihydroxy-7-methoxy-6,11-dioxo-1,2,3,4,6,11-hexahydrotetracen-2-yl)-2-hydroxyethylidene)-2,3,4,5,6-pentahydroxyhexanehydrazide (Glu-DOX)

Glu-NHNH$_2$ (361.4 mg, 1.72 mmol) in anhydrous DMSO (10.0 mL) was added dropwise to a solution of doxorubicin hydrochloride (500.0 mg, 0.86 mmol). The resulting solution was stirred at 25 ^oC for 0.5 h under an atmosphere of nitrogen. After evaporation of DMSO under reduced pressure, the resulting mixture was purified by reverse phase silica gel column chromatography (gradient 2 to 20 percent acetonitrile in water) to give the title compound (280.0 mg, 44.0%). ^1H NMR (400 MHz, DMSO-d_6) δ (ppm): 11.63 (s, 1H, NH), 8.02 (br, NH_2), 7.73-7.88 (m, 2H, CH), 7.62-7.51 (d, J = 7.58 Hz, 1H, CH), 6.07-5.94 (br, OH), 5.78-5.65 (br, OH), 5.56-5.36 (br, OH), 5.37-5.21 (m, 1H, CH), 5.18-5.09 (br, OH), 5.09-4.98 (m, 1H, CH), 4.76-4.29 (br, CH_2 & OH), 4.24-4.08 (m, 2H, CH), 4.07-3.80 (m, 4H, CH & CH_3), 3.66-3.22 (m, 6H, CH & CH_2), 3.09-2.86 (m, 2H, CH_2), 2.35-2.01 (m, 2H, CH_2), 1.96-1.58 (br, 2H, CH_2), 1.26-1.14 (d, J = 1.19 Hz, 3H, CH_3). ^{13}C NMR (100 MHz, DMSO-d_6) δ (ppm): 186.63

(overlap, 2C), 169.16, 161.14, 158.56, 156.76, 155.15, 136.65, 136.21, 135.59, 134.98, 120.13 (overlap, 2C), 119.33, 110.83 (overlap, 2C), 99.78, 74.25, 72.79, 72.15, 72.02, 71.59, 70.56, 66.68, 66.60, 63.77, 57.72, 57.04, 47.07, 38.36, 33.40, 28.78, 17.30. HRMS: (ESI) $[M+H]^+$ calcd. for $C_{33}H_{41}N_3O_{16}$, 736.2565, found 736.2555.

2.8 Preparation of Lac-DOX and Glu-DOX nanoparticles

Briefly, Lac-DOX (5.0 mg) was dissolved in 5.0 mL methanol. The solution was evaporated in a pear-shaped flask under reduced pressure. Ultra pure water (5.0 mL) was added to the flask under ultrasonic field to produce a solution with a concentration of 1.0 mg/mL for further experiments. Glu-DOX nanoparticles were obtained following the same procedure.

2.9 Critical aggregation concentration (CAC) measurements

To investigate the aggregation of Lac-DOX, the CAC measurements were performed. Nile red in acetone was added to indicate concentrations of Lac-DOX in water and the concentration of nile red was fixed at 10 μM. The fluorescence emission intensity of wavelength at 620 nm was determined by means of excitation wavelength at 543 nm.

2.10 Preparation of Cy5.5-loaded Lac-DOX nanoparticles

4.0 mg Lac-DOX and 0.4 mg Cy5.5 were dissolved in 2.0 mL of DMSO. Then the mixture was added dropwise to 2.0 mL ultra pure water and stirred at 25 ^{o}C for 15 min. Subsequently the solution was dialyzed against ultra pure water for 12 h (molecular weight cutoff (MWCO) = 1,000 g/mol) and the ultra pure water was exchanged every 3 h. To determine the content of Cy5.5 in Lac-DOX nanoparticles, the solution was lyophilized and then redissolved in DMSO. The amount of Cy5.5 in Lac-DOX nanoparticles was determined by measuring the absorbance at 680 nm with a UV/Vis spectrophotometer, wherein a calibration curve was obtained with Cy5.5/DMSO solutions with different Cy5.5 concentrations.

2.11 *In vitro* acid-triggered drug release study

The release profiles of doxorubicin from Lac-DOX nanoparticles were studied at pH 5.5 and pH 7.4 in dialysis tubes with a MWCO of 3000 at 37 ^{o}C. At desired time intervals, 0.5 mL buffer solution

outside the dialysis bag was taken out for HPLC measurements and replenished with an equal volume of fresh media to keep the sink condition. The amount of doxorubicin was determined by an HPLC Agilent 1260 Infinity system (Agilent) using a 3/1 (V/V) mixture of methanol and water as a mobile phase.

2.12 Cell culture

SMMC-7721 cells (a human hepatocellular carcinoma cell line) were cultured in Dulbecco's Modified Eagle's medium (DMEM) containing 10% fetal bovine serum (FBS) and antibiotics (50 units/mL penicillin and 50 units/mL streptomycin) at 37 ^{o}C in a humidified atmosphere containing 5% CO_2.

2.13 Cellular uptake

Cellular uptake by SMMC-7721 cells was performed on flow cytometry and confocal laser scanning microscope (CLSM), respectively. For flow cytometry studies, approximately 5×10^5 SMMC-7721 cells were seeded in 6-well culture plates per well and cultured overnight, followed by removing culture medium and adding Lac-DOX nanoparticles (equivalent DOX concentration: 8 μg/mL) at 37 ^{o}C for predetermined time intervals. Thereafter, drug solutions were removed and the cells were washed three times with PBS and treated with trypsin. The cells were detached from cell culture. Then the solutions were centrifugated for 5 min (1000 rpm). After the supernates were removed, the cells were resuspended in 0.5 mL of PBS. A single cell suspension was prepared by filtration through a 300 mesh filter. Finally, data for 1×10^4 gated events were collected by means of a flow cytometry on a LSRFortessa (BD) and analyzed by BD FACSDiva software. For CLSM studies, SMMC-7721 cells were seeded in 12-well culture plates (a clean coverslip was put in each well) at 2×10^5 cells per well in 1 mL of complete DMEM and grown overnight, followed by removing culture medium and adding Lac-DOX nanoparticles (equivalent DOX concentration: 8 μg/mL) at 37 ^{o}C for predetermined time intervals. The supernatant was carefully removed and the cells were washed with ice-cold PBS three times. Subsequently, the cells were fixed with 4% formaldehyde in each well for 30 min at room temperature and washed three times with ice-cold PBS again. Finally, Hoechst 33342 fluorescence dye was added to every sample for 15 min to stain the cell nuclei. The slides were rinsed with PBS for three

times. The slides were mounted and observed by a Nikon Ti-E inverted motorized microscope with a Nikon A1Si spectral detector confocal system running NIS-C Elements software.

2.14 *In vitro* cell proliferation assay

SMMC-7721 cells were plated in 96-well plates at 8×10^3 cells per well and further incubated for 24 h. The medium was removed and serial dilutions of DOX·HCl or Lac-DOX nanoparticles were added to cells. The cells were grown for another 48 h. Then, MTT was used for mitochondrial activity evaluation in cell viability studies. The medium was removed carefully after the cells were incubated for 4 h. The obtained blue formazan crystals were dissolved in 200 μL DMSO per well, and the absorbance was measured in a Perkin-Elmer 1420 Multilabel counter at a wavelength of 490 nm.

2.15 Cell apoptosis assay

Apoptosis in cells was visualized using an Alexa Fluor® 488 annexin V/Dead cell apoptosis kit according to the manufacturer's protocol. Briefly, SMMC-7721 cells were plated in 6-well plates at 5×10^5 cells per well and further incubated for 24 h. Apoptosis in cells was induced by treating cells with DOX·HCl or Lac-DOX nanoparticles at equivalent DOX concentration (2 μg/mL) for 12 h. A negative control was prepared by incubating cells in the absence of inducing agent. Cells were harvested, washed twice with cold PBS and stained with Alexa Fluor® 488 annexin V and PI according to the manufacturer's instructions. The stained cells were analyzed by a flow cytometry on a LSRFortessa (BD).

2.16 Animals

All male Balb/c nude mice (18-20 g) and SD rats (~200 g) were purchased from Chinese Academy of Sciences (Shanghai, China). Animal studies were conducted in accordance with the guidelines for the care and use of laboratory animals proved by the Animal Ethics Committee of Shanghai Jiao Tong University. SMMC-7721 cells were injected subcutaneously in flanks of male Balb/c nude mice at 2×10^6 cells per tumor. The tumors were allowed to grow for around 50 mm^3 and 250 mm^3 for antitumor studies and *in vivo* optical imaging experiments, respectively.

2.17 *In vivo* antitumor studies

The tumor bearing nude mice as described above were randomly divided into three cohorts of six mice each. Lac-DOX nanoparticles and free DOX·HCl were intravenously injected via the tail vein at a dose of 10 mg/kg (200 μL) every three days for 27 days. The control group only received saline (200 μL). The width and length of the tumors and the body weight of mice were measured at the time of each treatment. Tumor volume (V) was calculated using the following equation: V (mm^3) = 1/2 × length (mm) × width (mm) × width (mm). One mouse in each group was sacrificed on day 18. Tumors as well as major organs (heart, liver, spleen, lung and kidney) were dissected, weighted, sectioned into around 3 mm slices and fixed in 4% paraformaldehyde overnight for histology and immunohistochemical analysis.

2.18 Histology and immunohistochemical analyses

For histology analysis, tumors and major organs were treated according to the routine histological procedures. Briefly, they were embedded in paraffin. The paraffin embedded tumors and organs were cut at 5 μm thickness. Sections were subsequently stained with hematoxylin solution and eosin Y solution (H & E) to assess histological alterations by microscope (Nikon ECLIPSE Ti). For immunohistochemical analysis, the paraffin-embedded 5-μm-thick tumor sections were mounted on glass slides. Tissue sections were deparaffinized in xylene, rehydrated in graded alcohols (100%, 95%, 85%, 75%) and washed in distilled water. Endogenous peroxidase was blocked by 3% hydrogen peroxide aqueous solution for 10 min, and the slides were heated to boil in EDTA Antigen Retrieval Solution for 10 min by using water bath for antigen retrieval. Thereafter, the sections were cooled, rinsed twice with PBS. Non-specific bonding sites were blocked with goat serum in TBS for 20 min. The sections were incubated for 1 h with PCNA antibody (1:100) at room temperature. Then, the slides were rinsed three times with PBS and incubated for 1 h with a goat anti-mouse HRP secondary antibody at a dilution of 1:1000 followed by colorimetric detection using DAB. Finally, the sections were counterstained with hematoxylin and prepared for mounting. Images were taken on a Nikon ECLIPSE Ti microscope.

2.19 *In vivo* optical imaging and *ex vivo* biodistribution studies

In vivo optical imaging was conducted and analyzed using a Kodak multimode imaging system with 690 nm excitation wavelength and 700 nm emission wavelength. The tumor bearing nude mice were anesthetized with 4% chloral hydrate. Cy5.5-loaded Lac-DOX nanoparticles and free Cy5.5 were injected through the vein tail and imaging was performed at 1, 2, 3, 4 and 8 h postinjection. For the *ex vivo* biodistribution study, the tumor bearing nude mice were injected with Lac-DOX nanoparticles and free DOX·HCl (10 mg/kg bw).Tumor tissues and major organs were carefully harvested at 1, 2 and 8 h postinjection. All samples were rinsed with saline and immediately imaged using a Kodak multimode imaging system.

2.20 Pharmacokinetics

To determine the pharmacokinetics profiles of Lac-DOX nanoparticles and free DOX·HCl, SD rats (~200 g) were randomly divided into 2 groups (n = 4). Drugs were intravenously injected through tail vein at a dose of 10 mg/kg. The blood samples (0.2 mL) were collected via eye puncture at the time point of 5 min, 15 min, 30 min, 1 h, 2 h, 4 h, 6 h, 8 h, 10 h, and 12 h. Blood samples were processed for serum by centrifugation (10 min, 1000 rpm) to determine the pharmacokinetics property of Lac-DOX nanoparticles and free DOX·HCl.

2.21 Blood biochemistry assay

The tumor bearing nude mice were intravenously injected via the tail vein at a dose of 10 mg/kg (200 μL) every three days for 15 days. The blood samples were collected via eye puncture for blood biochemistry assay.

3. Results and discussions

3.1 Synthesis of Lac-DOX and Preparation of Lac-DOX nanoparticles

The synthesis and self-assembly of Lac-DOX are showed in Scheme 2, and the details are described in Methods. Briefly, lactobionolactone was first synthesized via the lactonization of lactobionic acid. Lactobionolactone was then converted to Lac-$NHNH_2$ by hydrazinolysis. Lac-$NHNH_2$ reacted with

doxorubicin hydrochloride (DOX•HCl) to produce Lac-DOX. The structure of Lac-DOX was confirmed by ^{1}H and ^{13}C NMR. As shown in Fig. 1, the proton signal at 11.68 ppm (1) belongs to the secondary amine of the acylhydrazone group and the proton signals at 6.15-5.96 ppm and 5.65-4.42 ppm belong to the hydroxyl protons of Lac in the ^{1}H NMR spectrum of Lac-DOX. Besides, the carbon signal at 214.57 ppm (2) corresponding to the carbonyl group of DOX disappears, and a new peak appears at 158.53 ppm (2') corresponding to R_1R_2C=NNH- group of Lac-DOX in the ^{13}C NMR spectrum. Lac-DOX was also characterized by ultraviolet/visible spectrophotometer (UV/Vis), Fourier transform infrared spectroscopy (FTIR), fluorescence spectroscopy (Figs. S3-S5) and high-resolution mass spectra (HRMS). All experimental results demonstrate that Lac-DOX has been synthesized successfully. For comparison, delta-gluconolactone doxorubicin conjugate (Glu-DOX) was synthesized using the method of two steps (Fig. S1) by reaction of hydrazine hydrate with delta-gluconolactone to synthesize Glu-$NHNH_2$ and then by reaction of Glu-$NHNH_2$ with DOX•HCl to produce Glu-DOX (Fig. S2).

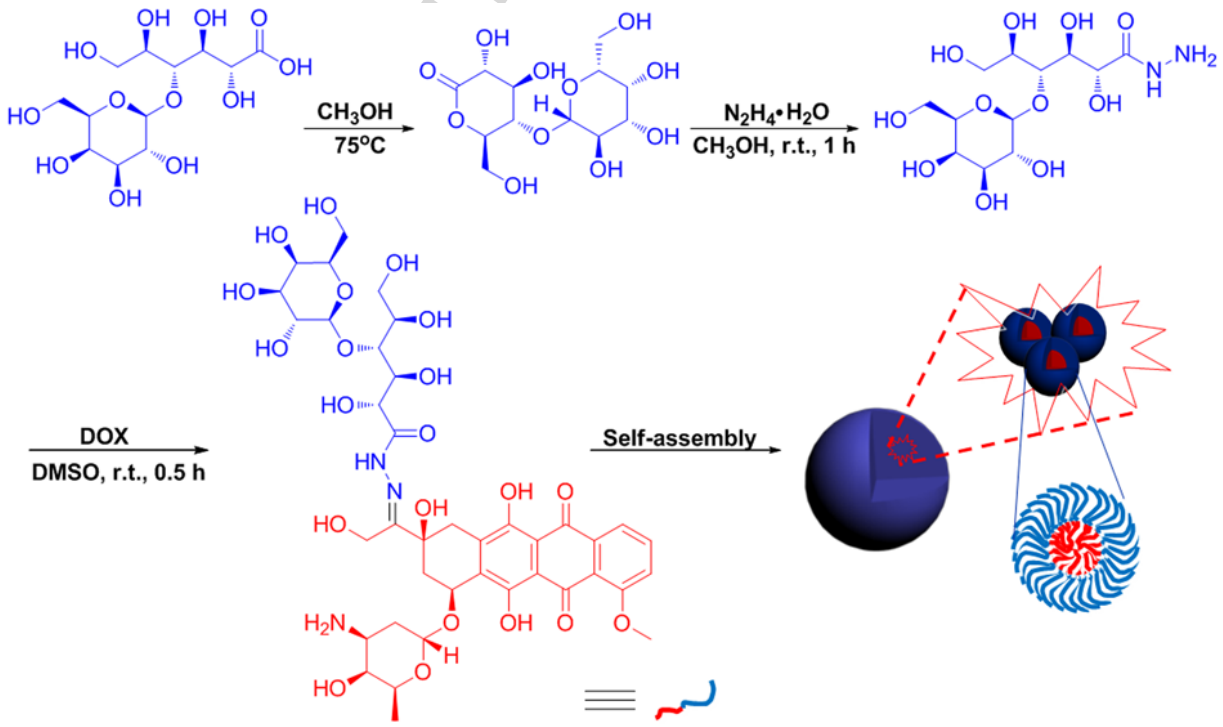

Scheme 2. Synthesis Route of Lac-DOX and Schematic Representation of the Self-Assembled Lac-DOX Nanoparticles.

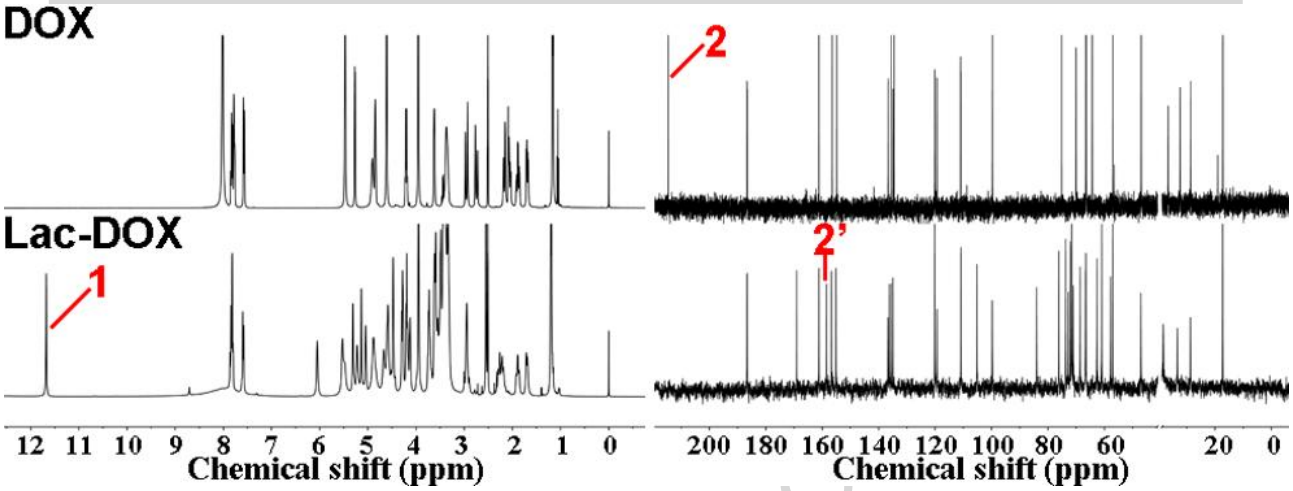

Fig. 1. ^{1}H NMR and ^{13}C NMR spectra of DOX and Lac-DOX. 1: the proton signal of the secondary amine of the acylhydrazone group (Lac-DOX), 2: the carbon signal of the carbonyl group (DOX), 2': the carbon signal of R_1R_2C=NNH- group (Lac-DOX). (Note: The signal of the ^{13}C NMR spectra around 40 ppm is the solvent peak of DMSO.)

Due to its amphiphilicity, Lac-DOX self-assembled into nanoparticles in water. As shown in Fig. 2a, the average hydrodynamic diameter of Lac-DOX nanoparticles is about 172.8 nm determined by DLS. The morphology of the nanoparticles was observed by transmission electron microscopy (TEM). The average diameter of these spherical nanoparticles consisting of a lot of small spherical domains is approximate 150 nm from the TEM image in Fig. 2b, which is consistent with the DLS results. We infer that these nanoparticles are a type of multi-micelles aggregates (MMA), which has already been well reported [38, 47]. The CAC measurements were performed to investigate the self-assembly behavior of Lac-DOX by using Nile Red as a fluorescent probe. Nile Red does not emit fluorescence in aqueous solution, but its fluorescence is known to increase substantially in the hydrophobic environments of micelles [48-51]. The fluorescence intensities were monitored by adding different amounts of Lac-DOX into an aqueous dispersion of Nile Red (10 μM). Fig. S7 shows the observed inflection point corresponding to a CAC of 2 μg/mL, indicating the rather high stability of Lac-DOX nano-particles [52].

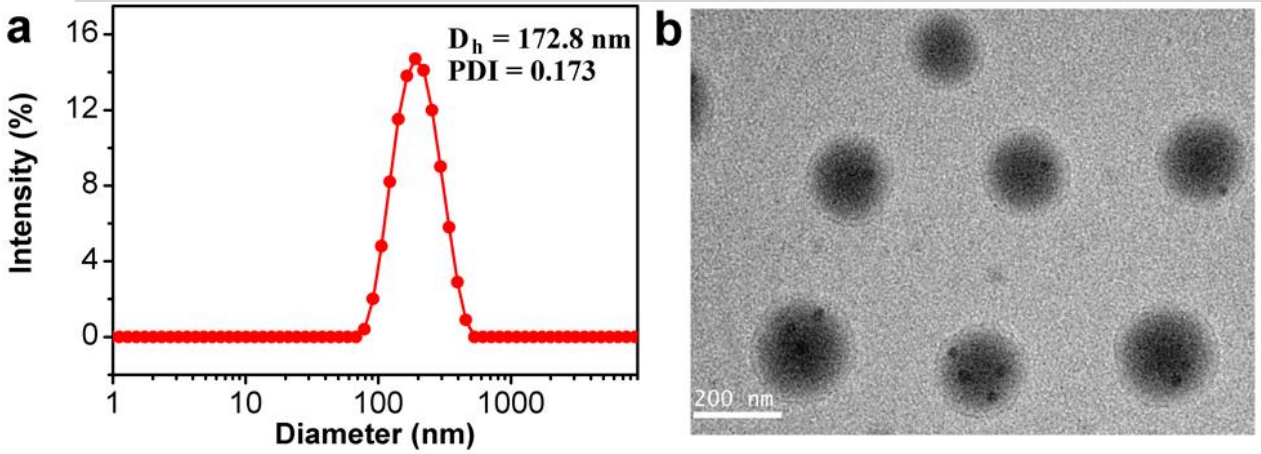

Fig. 2. (a) DLS profile of Lac-DOX nanoparticles, the average size (Dh = 172.8 nm) and the polydispersity index (PDI = 0.173). (b) TEM image of Lac-DOX nanoparticles. Scale bars: 200 nm.

3.2 *In Vitro* Drug Release

As a pH-responsive molecule, Lac-DOX could be hydrolyzed to lactobionic acid and DOX at an acidic pH. Lac-DOX nanoparticles were incubated under different pH conditions (pH 7.4 and 5.5) corresponding to the pH of blood and late endosome [53]. An aliquot of the Lac-DOX nanoparticles was taken out for HPLC measurements at predetermined time intervals. As shown in Fig. S6, almost all of DOX is released at pH 5.5 after 24 h incubation, while little DOX is released within 24 h at pH 7.4. The release profiles indicate that Lac-DOX nanoparticles remain stable in the blood circulation and normal extracellular environment, while DOX can be rapidly released under endo/lysosomes conditions of cancer cells.

3.3 *In Vitro* Studies of Lac-DOX Nanoparticles

To investigate the proliferation inhibition of SMMC-7721 cells (a human hepatocellular carcinoma cell line) induced by Lac-DOX nanoparticles and free DOX, MTT assay was used and the details are described in the Supporting Information. Fig. 3a shows that the cytotoxicity of Lac-DOX to SMMC-7721 cells is nearly the same as that of free DOX, indicating that Lac-DOX and free DOX almost have the same anticancer ability *in vitro*. It can be attributed to the fast release of free DOX from the Lac-DOX nanoparticles (Fig. S6).

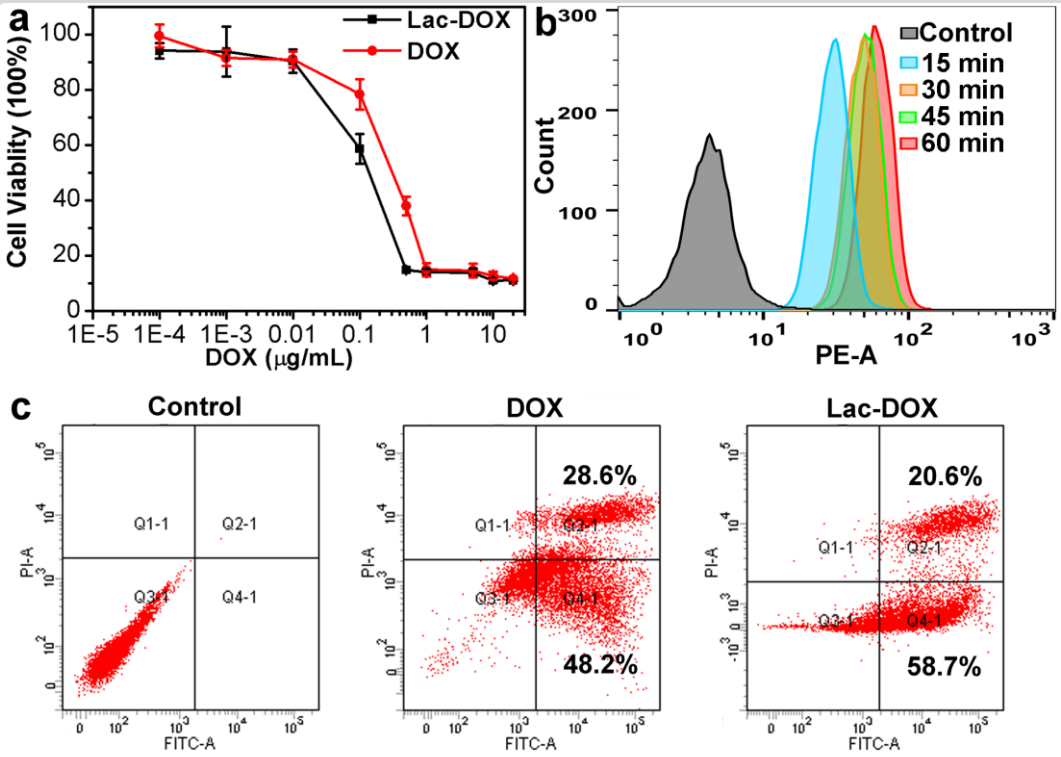

Fig. 3. (a) Cell viability of SMMC-7721 cells against Lac-DOX nanoparticles or DOX after culture for 48 h. (b) In vitro cellular uptake studies of Lac-DOX nanoparticles in SMMC-7721 cells determined by FCM. (c) Apoptosis was evaluated following treatment of SMMC-7721 cells induced by DOX or Lac-DOX nanoparticles at equivalent DOX concentration (2 μg/mL) for 12 h, by staining with Annexin V-FITC & PI. Early apoptotic cells are presented in the Lower right quadrant, and late apoptotic cells are presented in the upper right quadrant.

Cellular uptake behaviors of Lac-DOX nanoparticles were investigated by FCM and CLSM against SMMC-7721 cells. Fig. 3b shows the mean fluorescence intensity of the aromatic chromophore of DOX after incubation with Lac-DOX nanoparticles for 15, 30, 45 and 60 min. The intracellular DOX fluorescence increases with increasing incubation time, which can be attributed to the cellular uptake of Lac-DOX nanoparticles by SMMC-7721 cells. The outcome of CLSM (Fig. S10) is consistent with the FCM results. The nucleus region was stained into blue by Hoechst 33342. Here, the red fluorescence is emitted from free DOX or Lac-DOX. As shown in Fig. S10, free DOX, a small molecular anticancer drug, can rapidly diffuse into the nucleus regions of SMMC-7721 cells within 15 min. While for

Lac-DOX nanoparticles, the red fluorescence of nucleus region gradually increases with the accumulation of DOX from Lac-DOX nanoparticles.

As a fundamental biological phenomenon, apoptosis plays a crucial role in normal tissue homeostasis. To induce apoptosis is also a common way to treat cancer [54-56]. For example, many anticancer drugs (e.g., DOX) kill cancer cells primarily by inducing apoptosis. Annexin V, which has a high affinity for phosphatidyl serine, labeled with fluorescein isothiocyanate (FITC) can identify apoptotic cells by binding to phosphatidyl serine exposed on the outer leaflet. Propidium iodide (PI) binding tightly to the nucleic acids in the cell specifically stains dead cells with red fluorescence. Thus the SMMC-7721 cells treated by free DOX and Lac-DOX nanoparticles were probed by Annexin V-FITC & PI assay and analyzed by flow cytometry (FCM) to further quantify the cell apoptosis [57, 58]. As illustrated in Fig. 3c, the percentages of the apoptosis cells are 76.8% and 79.3% in free DOX and Lac-DOX nanoparticle groups, respectively, which is quite consistent with the result of MTT assay. Both MTT and apoptosis results indicate that Lac-DOX nanoparticles and free DOX almost have the same capability to inhibit the growth of SMMC-7721 cells.

3.4 Passive and active targeting behaviors of Lac-DOX

Galactosyl has a specific interaction with the asialoglycoprotein (ASGP) receptors over-expressed on hepatocyte membranes [59, 60]. Lac is a disaccharide sugar derived from galactose and glucose. Thus Lac-DOX nanoparticles are expected to have liver-targeting ability. To evaluate the active-targeting efficiency of Lac-DOX nanoparticles, galactose-free Glu-DOX nanoparticles were used as control. SMMC-7721 cells were incubated with Lac-DOX nanoparticle solution and Glu-DOX nanoparticle solution (equivalent DOX concentration: 8 μg/mL) for predetermined time intervals, respectively. The mean fluorescence intensity of DOX was determined by FCM. As shown in Fig. 4a, although the equivalent DOX concentration is used, the SMMC-7221 cells incubated with Lac-DOX nanoparticles display much higher fluorescence intensity than those with Glu-DOX nanoparticles. It indicates that Lac-DOX can actively target SMMC-7721 cells by specifically interacting with the ASGP receptors.

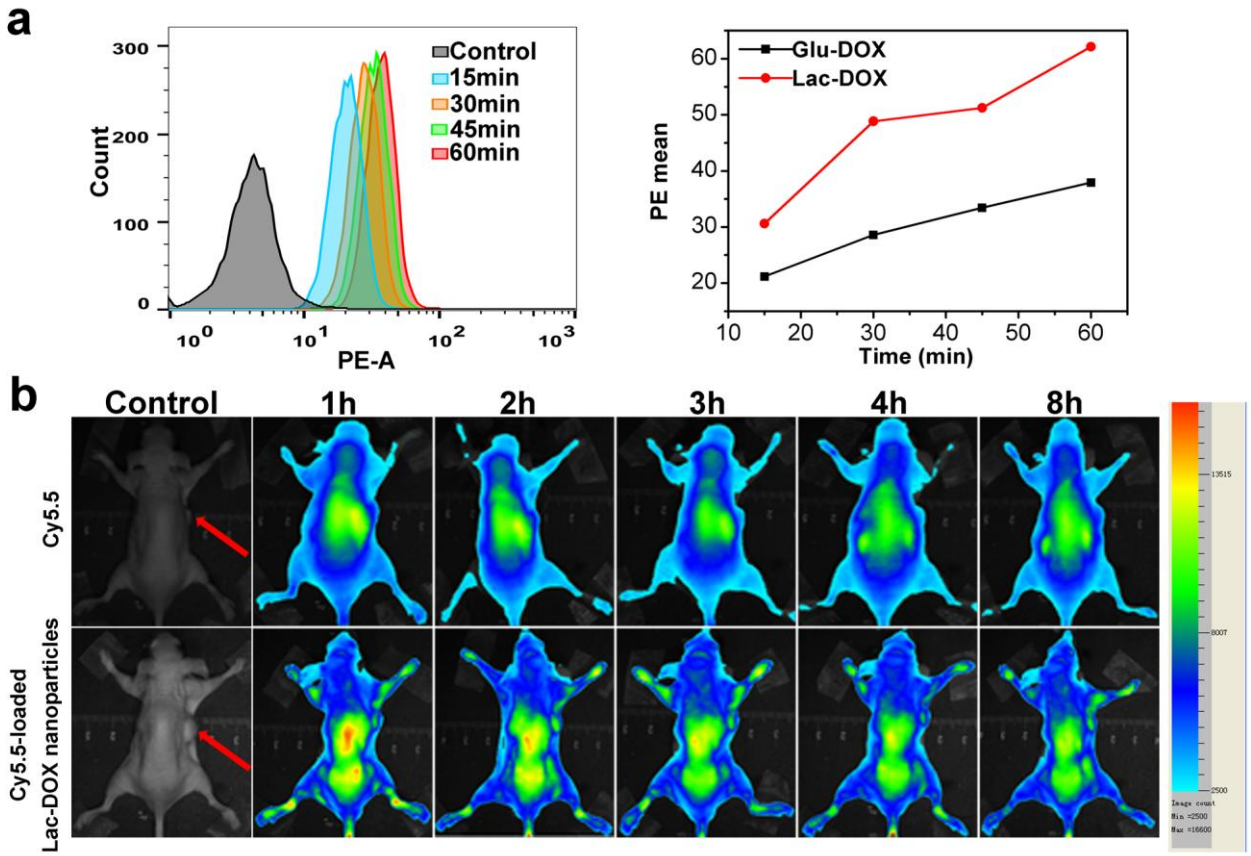

Fig. 4. The active and passive target behaviors of Lac-DOX nanoparticles. (a) Non-liver-targeting Glu-DOX nanoparticles (the left fig.), and the right fig. showed the time-dependent profiles of Lac-DOX nanoparticles and Glu-DOX nanoparticles mean fluorescence intensity in SMMC-7721 cells. (b) In vivo imaging of the tumor-bearing nude mice was performed after intravenous injection of free Cy5.5 or Cy5.5-loaded Lac-DOX nanoparticles. The fluorescence images were acquired at post-injection with 1 h, 2 h, 3 h, 4 h and 8 h.

To investigate whether Lac-DOX nanoparticles could passively target tumor sites via the EPR effect, *in vivo* optical imaging was conducted. The Cy5.5-loaded Lac-DOX nanoparticles were prepared for real-time *in vivo* imaging. These nanoparticles and free Cy5.5 were injected intravenously into the tumor bearing nude mice. The fluorescence signals of Cy5.5 were recorded on a Kodak multimode imaging system at 1, 2, 3, 4 and 8 h postinjection. Fig. 4b shows that during the whole time observation, the fluorescence of free Cy5.5 remains weak at the tumor site, while the fluorescence signal of Cy5.5-loaded Lac-DOX nanoparticles appears at the tumor site at 1 h postinjection. Even 8 h after

injection the fluorescence signal still remains strong, confirming the accumulation of Lac-DOX nanoparticles in the tumor. The accumulation of Lac-DOX nanoparticles can be attributed to the EPR effect. The nanoparticles with suitable size are trapped due to the tortuous and leaky vasculatures in the tumor. The cellular uptake behaviors of Lac-DOX nanoparticles against SMMC-7721 cells and *in vivo* optical imaging results indicate that Lac-DOX nanoparticles can target liver tumor both actively and passively.

3.5 *In vivo* antitumor studies

To investigate the therapeutic efficiency of Lac-DOX nanoparticles *in vivo*, the athymic nude mice bearing human hepatoma SMMC-7721 cells were used. The tumor volume reached about 50 mm^3 in one week. Therapeutic details are shown in the Supporting Information. The width and length of the tumors and the body weight of mice were measured before the time of each treatment. As illustrated in Fig. 5a, the therapeutic efficiency of free DOX and Lac-DOX nanoparticles is comparable till day 9. The therapeutic efficiency of Lac-DOX nanoparticles is a little lower than that of free DOX between day 12 and day 15, which can be attributed to the dramatic decrease in body weight of DOX-treated group (Fig. 5c), leading to the deceptive therapeutic effect. Owing to severe side effects of DOX causing the death of DOX-treated group, no therapeutic data of DOX-treated group is recorded after day 15. However, the tumor growth of Lac-DOX nanoparticle treated group is inhibited (Fig. 5a) and the mean body weight has no significant change compared with the control group (Fig. 5c). These results demonstrate that the therapeutic effects of free DOX and Lac-DOX nanoparticles are comparable, which are consistent with the results of experiments. In the meantime, Lac-DOX nanoparticles show weak side effects on the tumor-bearing nude mice (Figs. 5b and 5c).

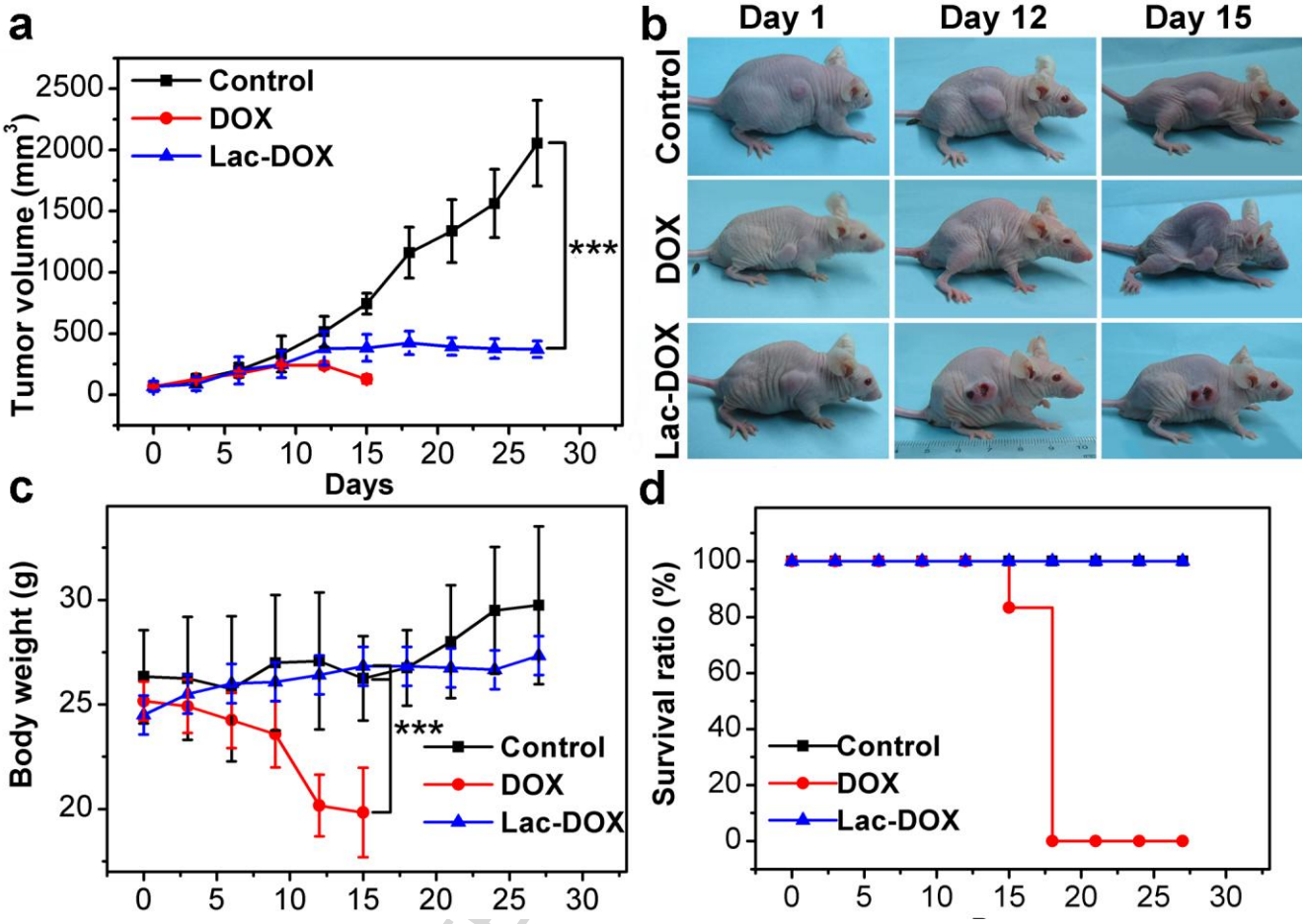

Fig. 5. In vivo therapeutic efficacy of Lac-DOX nanoparticles in the athymic nude mice bearing human hepatoma SMMC-7721 cells. (a) Tumor volumes of each group were recorded after intravenous injection of saline, free DOX and Lac-DOX nanoparticles (n = 6 in each group). The tumor volumes were normalized to their initial sizes. Statistical significance: *P < 0.05, **P < 0.01 and ***P < 0.001. (b) Photographs of the tumor-bearing nude mice after treatment on day 1, day 12 and day15. (c) Body weight changes of the tumor-bearing mice during the experiments. (d) Survival curves of the tumor-bearing mice with indicated treatments.

3.6 Pharmacokinetics

Compared with small molecular drugs, nanoparticles with suitable size exhibit improved pharmacokinetic properties in the bloodstream. The serum DOX and Lac-DOX concentration-time profiles are illustrated in Fig. 6c. The concentration of Lac-DOX is much higher than that of free DOX at the same time up to 10 h. These results show that compared with free DOX the clearance of

Lac-DOX nanoparticles is slow down due to their nanoscale characteristics in the bloodstream. To further confirm the above results, the *ex vivo* biodistribution study, histology analysis, immunohistochemical analysis and serum biochemistry assays were performed.

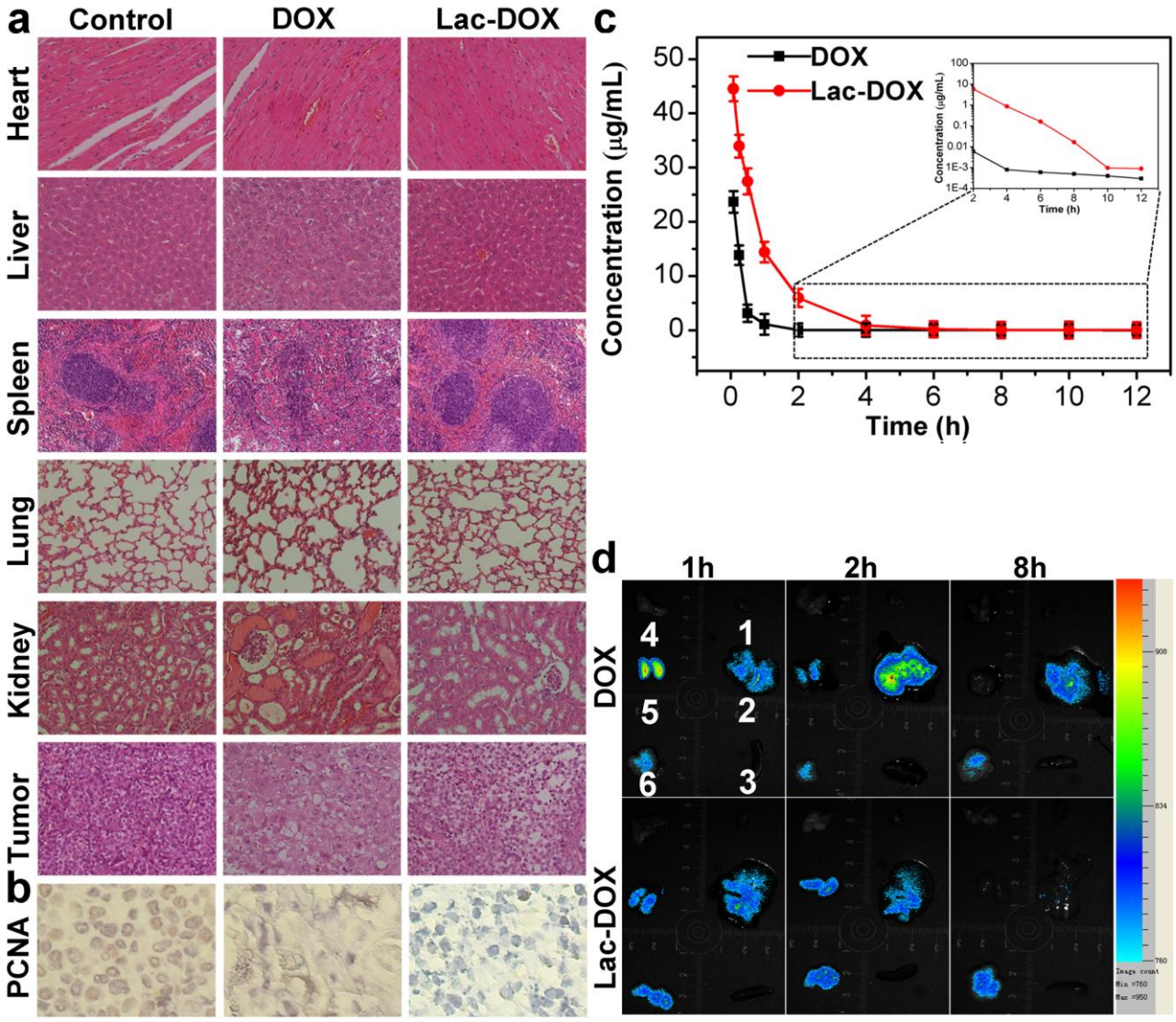

Fig. 6. (a) Microscopic images of H&E-stained sections of the major organs and tumors (on day 18). (b) Immunohistochemical analysis of tumors by PCNA antibody. The tumor tissues were harvested after 15 days of treatment. (c) In vivo pharmacokinetics profiles of drugs in SD rats (n = 4 in each group). (d) Images of the major organs and tumors harvested at 1, 2 and 8 h postinjection. 1 heart, 2 liver, 3 spleen, 4 lung, 5 kidneys, 6 tumor.

3.7 *Ex vivo* biodistribution study

For the *ex vivo* biodistribution study, tumor tissues and major organs (heart, liver, spleen, lung,

kidney) were carefully excised at different time intervals and the fluorescence of the aromatic chromophore of DOX was monitored. As shown in Fig. 6d, Lac-DOX nanoparticles mainly accumulate in the tumor site during the whole time observed. The fluorescence signals in major organs are relatively weak, indicating the weak side effects of Lac-DOX nanoparticles. While for free DOX, the fluorescence signals measured at tumor site become weaker and weaker in a short time. In major organs it mainly accumulates in the kidney at 1 h postinjection. Then free DOX accumulates in the liver at 2 h postinjection. At 8 h postinjection the signals of free DOX can still be detected in the liver. The long time accumulation of free DOX in major organs may cause severe side effects.

3.8 Histology and immunohistochemical analyses

The accumulation of free DOX in the liver and kidneys might cause some side effects. Thus the major organs and tumors were harvested on day 18 for histology (Fig. 6a) and immunohistochemical (Fig. 6b) analyses. The tumors and major organs were treated according to the routine histological procedures. Comparing with the PBS control group, the major organs of Lac-DOX nanoparticle group show no tissue damage. While for free DOX-treated group, the spleens and kidneys are severely damaged. The morphology of tumor cells is obviously changed except for the PBS control group. Then the proliferating cell nuclear antigen (PCNA) images were used to study the proliferation of tumor cells. PCNA-positive nuclei were brown, and PCNA-negative nuclei were blue. The nucleus of the PBS control group was stained by brown. However, most tumor cells of free DOX group and Lac-DOX nanoparticle group were blue. These results are quite compatible with that of *in vivo* antitumor studies. That is to say Lac-DOX nanoparticles show comparable antitumor activity compared with free DOX. However, no obviously side effects are observed for Lac-DOX nano-particle group.

3.9 Blood biochemistry assay

Besides, the blood biochemistry indexes were also measured to assess the toxicities from DOX. As shown in Fig. 7, blood urea nitrogen (Urea) and creatinine (Cr) of Lac-DOX nanoparticle group do not show significant difference with control group. But for free DOX group, the Urea value is obviously lower than that of control group, indicating that obvious hepatic or kidney dis-order[61] is induced by

free DOX.

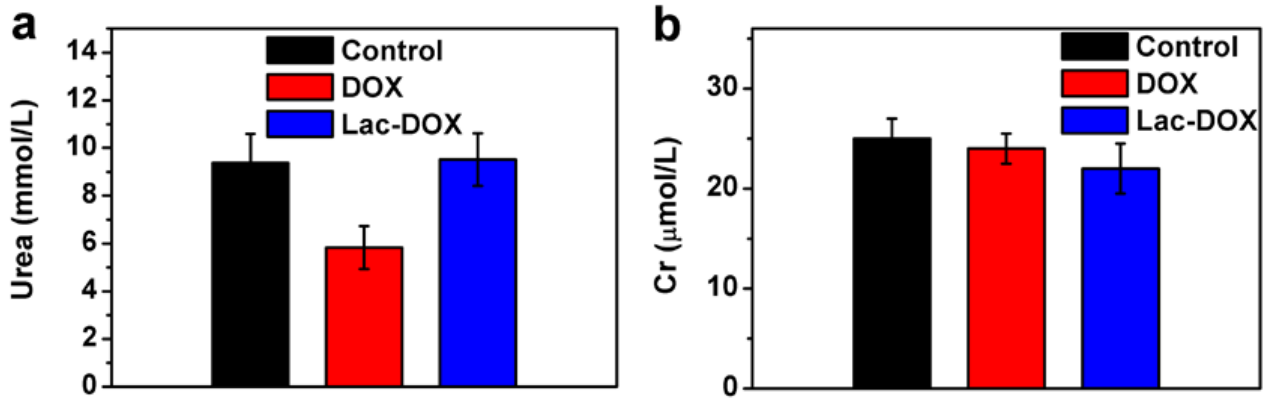

Fig. 7. Blood biochemical indexes of SMMC-7721 tumor-bearing nude mice after free DOX and Lac-DOX nanoparticle treatments. Mean and standard deviation of blood urea nitrogen (Urea) and creatinine (Cr) of SMMC-7721 tumor-bearing nude mice (n = 5).

4. Conclusions

ADDC combines the advantages of highly potent anticancer drugs and long blood circulation time together without carriers. However, the toxic anticancer drug moieties of ADDC are aggregated not only in the core but also in the surface of the micelles, which may lead to undesired toxicities during the blood circulation. Besides, the targeted ability of ADDC is limited only through EPR effect. Making use of the advantages and bypassing some disadvantages of ADDC, here we have developed a novel kind of active targeting nanodrug delivery system, which is fabricated via conjugating targeting ligand such as Lac to chemotherapy drug such as DOX by a facile way with on-demand drug release behavior. Different from nanocarrier-based drug delivery systems, the annoying problems from the degradation, metabolism and excretion of carriers can be completely eliminated in our system. For Lac-DOX conjugate, the drug loading efficiency is 61.7%, which is tremendously high. Benefiting from its amphiphilicity, Lac-DOX conjugate self-assembles into nanoparticles with suitable size. At an

endosome/lysosome acidic environment, DOX is completely released from Lac-DOX nanoparticles within 24 h. The anticancer activity of Lac-DOX nanoparticles is assessed both *in vitro* and *in vivo*. The cell proliferation assay and apoptosis assay indicate that Lac-DOX nanoparticles and free DOX almost have the same capability to inhibit the growth of SMMC-7721 cells. In addition, due to their improved pharmacokinetic properties and passive and active tumor targeting abilities, Lac-DOX nanoparticles mainly accumulate at the tumor site with enhanced cellular uptake. Besides, the lower uptake of Lac-DOX in major organs, normal body weights and normal blood biochemistry indexes indicate that Lac-DOX nanoparticles show very weak side effects *in vivo*. Consequently, this kind of active targeting nanodrug delivery system consisting of amphiphilic targeting ligand-chemotherapy drug conjugates would open the doors to a new strategy for cancer therapy.

Acknowledgments

The authors thank the National Basic Research Program (2015CB931801) and the National Natural Science Foundation of China (51473093). We thank Lei Feng (Instrumental Analysis Center of Shanghai Jiao Tong University) for HRMS assay, Yue Su and Linzhu Zhou for in vitro experiments and Bing Liu and Dali Wang for in vivo experiments. We are also grateful to Mo Sun for an enlightening discussion.

Author information

Corresponding authors: Tel.: +86-21-54742664; Fax: +86-21-54741297; Correspondence and requests for materials should be addressed to D. Y. (dyyan@sjtu.edu.cn) or to X. Z. (xyzhu@sjtu.edu.cn**).** The authors declare no competing financial interests.

[1] Both authors contributed equally to this manuscript.

References

[1] M. Jang, J.H. Kim, H.Y. Nam, I.C. Kwon, H.J. Ahn, Design of a platform technology for systemic delivery of siRNA to tumours using rolling circle transcription, Nat. Commun., 6 (2015).

[2] K. Lee, M. Rafi, X. Wang, K. Aran, X. Feng, C. Lo Sterzo, R. Tang, N. Lingampalli, H.J. Kim, N. Murthy, In vivo delivery of transcription factors with multifunctional oligonucleotides, Nat. Mater., 14 (2015) 701-706.
[3] T.G. Park, J.H. Jeong, S.W. Kim, Current status of polymeric gene delivery systems, Adv. Drug Del. Rev., 58 (2006) 467-486.
[4] X. Guo, L. Huang, Recent advances in nonviral vectors for gene delivery, Acc. Chem. Res., 45 (2012) 971-979.
[5] R.M. Schiffelers, G.A. Koning, T.L.M. Ten Hagen, M.H.A.M. Fens, A.J. Schraa, A.P.C.A. Janssen, R.J. Kok, G. Molema, G. Storm, Anti-tumor efficacy of tumor vasculature-targeted liposomal doxorubicin, J. Control. Release, 91 (2003) 115-122.
[6] K.A. Carter, S. Shao, M.I. Hoopes, D. Luo, B. Ahsan, V.M. Grigoryants, W. Song, H. Huang, G. Zhang, R.K. Pandey, J. Geng, B.A. Pfeifer, C.P. Scholes, J. Ortega, M. Karttunen, J.F. Lovell, Porphyrin–phospholipid liposomes permeabilized by near-infrared light, Nat. Commun., 5 (2014).
[7] T. Nomoto, S. Fukushima, M. Kumagai, K. Machitani, Arnida, Y. Matsumoto, M. Oba, K. Miyata, K. Osada, N. Nishiyama, K. Kataoka, Three-layered polyplex micelle as a multifunctional nanocarrier platform for light-induced systemic gene transfer, Nat. Commun., 5 (2014).
[8] J. Liu, W. Huang, Y. Pang, P. Huang, X. Zhu, Y. Zhou, D. Yan, Molecular self-assembly of a homopolymer: An alternative to fabricate drug-delivery platforms for cancer therapy, Angew. Chem., Int. Ed., 50 (2011) 9162-9166.
[9] Y. Zhou, W. Huang, J. Liu, X. Zhu, D. Yan, Self-assembly of hyperbranched polymers and its biomedical applications, Adv. Mater., 22 (2010) 4567-4590.
[10] H. Wei, R.X. Zhuo, X.Z. Zhang, Design and development of polymeric micelles with cleavable links for intracellular drug delivery, Prog. Polym. Sci., 38 (2013) 503-535.
[11] H.Y. Tian, C. Deng, H. Lin, J. Sun, M. Deng, X. Chen, X. Jing, Biodegradable cationic PEG-PEI-PBLG hyperbranched block copolymer: Synthesis and micelle characterization, Biomaterials, 26 (2005) 4209-4217.
[12] E. Jin, B. Zhang, X. Sun, Z. Zhou, X. Ma, Q. Sun, J. Tang, Y. Shen, E. Van Kirk, W.J. Murdoch, M. Radosz, Acid-active cell-penetrating peptides for in vivo tumor-targeted drug delivery, J. Am. Chem. Soc., 135 (2013) 933-940.
[13] J. Wang, W. Mao, L.L. Lock, J. Tang, M. Sui, W. Sun, H. Cui, D. Xu, Y. Shen, The role of micelle size in tumor accumulation, penetration, and treatment, ACS Nano, 9 (2015) 7195-7206.
[14] L. Zhang, R. Guo, M. Yang, X. Jiang, B. Liu, Thermo and pH dual-responsive nanoparticles for anti-cancer drug delivery, Adv. Mater., 19 (2007) 2988-2992.
[15] X. Hu, G. Liu, Y. Li, X. Wang, S. Liu, Cell-penetrating hyperbranched polyprodrug amphiphiles for synergistic reductive milieu-triggered drug release and enhanced magnetic resonance signals, J. Am. Chem. Soc., 137 (2015) 362-368.
[16] A. Rösler, G.W.M. Vandermeulen, H.A. Klok, Advanced drug delivery devices via self-assembly of amphiphilic block copolymers, Adv. Drug Del. Rev., 64 (2012) 270-279.
[17] K. Cai, X. He, Z. Song, Q. Yin, Y. Zhang, F.M. Uckun, C. Jiang, J. Cheng, Dimeric drug polymeric nanoparticles with exceptionally high drug loading and quantitative loading efficiency, J. Am. Chem. Soc., 137 (2015) 3458-3461.
[18] M.L. Viger, J. Sankaranarayanan, C. De Gracia Lux, M. Chan, A. Almutairi, Collective activation of MRI agents via encapsulation and disease-triggered release, J. Am. Chem. Soc., 135 (2013) 7847-7850.
[19] J.A. Hubbell, A. Chilkoti, Nanomaterials for drug delivery, Science, 337 (2012) 303-305.
[20] G. Sun, H. Cui, L.Y. Lin, N.S. Lee, C. Yang, W.L. Neumann, J.N. Freskos, J.J. Shieh, R.B. Dorshow, K.L. Wooley, Multicompartment polymer nanostructures with ratiometric dual-emission pH-sensitivity, J. Am. Chem. Soc., 133 (2011) 8534-8543.
[21] K. Fan, C. Cao, Y. Pan, D. Lu, D. Yang, J. Feng, L. Song, M. Liang, X. Yan, Magnetoferritin nanoparticles for targeting and visualizing tumour tissues, Nat. Nanotechnol., 7 (2012) 459-464.
[22] A. MaHam, Z. Tang, H. Wu, J. Wang, Y. Lin, Protein-based nanomedicine platforms for drug delivery, Small, 5 (2009) 1706-1721.

[23] H.J. Kim, S.M. Lee, K.H. Park, C.H. Mun, Y.B. Park, K.H. Yoo, Drug-loaded gold/iron/gold plasmonic nanoparticles for magnetic targeted chemo-photothermal treatment of rheumatoid arthritis, Biomaterials, 61 (2015) 95-102.
[24] J.L. Vivero-Escoto, I.I. Slowing, C.W. Wu, V.S.Y. Lin, Photoinduced intracellular controlled release drug delivery in human cells by gold-capped mesoporous silica nanosphere, J. Am. Chem. Soc., 131 (2009) 3462-3463.
[25] Y. Cheng, A.C. Samia, J.D. Meyers, I. Panagopoulos, B. Fei, C. Burda, Highly efficient drug delivery with gold nanoparticle vectors for in vivo photodynamic therapy of cancer, J. Am. Chem. Soc., 130 (2008) 10643-10647.
[26] S. Gai, P. Yang, C. Li, W. Wang, Y. Dai, N. Niu, J. Lin, Synthesis of magnetic, up-conversion luminescent, and mesoporous core-shell-structured nanocomposites as drug carriers, Adv. Funct. Mater., 20 (2010) 1166-1172.
[27] F. Chen, H. Hong, S. Goel, S.A. Graves, H. Orbay, E.B. Ehlerding, S. Shi, C.P. Theuer, R.J. Nickles, W. Cai, In vivo tumor vasculature targeting of CuS@MSN based theranostic nanomedicine, ACS Nano, 9 (2015) 3926-3934.
[28] M. Vallet-Regí, F. Balas, D. Arcos, Mesoporous materials for drug delivery, Angew. Chem., Int. Ed., 46 (2007) 7548-7558.
[29] A. Tzur-Balter, Z. Shatsberg, M. Beckerman, E. Segal, N. Artzi, Mechanism of erosion of nanostructured porous silicon drug carriers in neoplastic tissues, Nat. Commun., 6 (2015).
[30] R. Namgung, Y. Mi Lee, J. Kim, Y. Jang, B.H. Lee, I.S. Kim, P. Sokkar, Y.M. Rhee, A.S. Hoffman, W.J. Kim, Poly-cyclodextrin and poly-paclitaxel nano-assembly for anticancer therapy, Nat. Commun., 5 (2014).
[31] Y. Shen, E. Jin, B. Zhang, C.J. Murphy, M. Sui, J. Zhao, J. Wang, J. Tang, M. Fan, E. Van Kirk, W.J. Murdoch, Prodrugs forming high drug loading multifunctional nanocapsules for intracellular cancer drug delivery, J. Am. Chem. Soc., 132 (2010) 4259-4265.
[32] T. Sun, Y.S. Zhang, B. Pang, D.C. Hyun, M. Yang, Y. Xia, Engineered nanoparticles for drug delivery in cancer therapy, Angew. Chem., Int. Ed., 53 (2014) 12320-12364.
[33] R. Tong, H.D. Hemmati, R. Langer, D.S. Kohane, Photoswitchable nanoparticles for triggered tissue penetration and drug delivery, J. Am. Chem. Soc., 134 (2012) 8848-8855.
[34] Y. Matsumura, H. Maeda, A new concept for macromolecular therapeutics in cancer chemotherapy: Mechanism of tumoritropic accumulation of proteins and the antitumor agent smancs, Cancer Res., 46 (1986) 6387-6392.
[35] J. Shi, A.R. Votruba, O.C. Farokhzad, R. Langer, Nanotechnology in drug delivery and tissue engineering: From discovery to applications, Nano Lett., 10 (2010) 3223-3230.
[36] S.M. Moghimi, A.C. Hunter, J.C. Murray, Nanomedicine: Current status and future prospects, FASEB J., 19 (2005) 311-330.
[37] M.E. Davis, Z. Chen, D.M. Shin, Nanoparticle therapeutics: An emerging treatment modality for cancer, Nat. Rev. Drug Discov., 7 (2008) 771-782.
[38] P. Huang, D. Wang, Y. Su, W. Huang, Y. Zhou, D. Cui, X. Zhu, D. Yan, Combination of small molecule prodrug and nanodrug delivery: Amphiphilic drug-drug conjugate for cancer therapy, J. Am. Chem. Soc., 136 (2014) 11748-11756.
[39] A. Kobayashi, T. Akaike, K. Kobayashi, H. Sumitomo, Enhanced adhesion and survival efficiency of liver cells in culture dishes coated with a lactose‐carrying styrene homopolymer, Die Makromo. Chem., Rapid Commun., 7 (1986) 645-650.
[40] K.K. Selim, Y.-S. Ha, S.-J. Kim, Y. Chang, T.-J. Kim, G.H. Lee, I.-K. Kang, Surface modification of magnetite nanoparticles using lactobionic acid and their interaction with hepatocytes, Biomaterials, 28 (2007) 710-716.
[41] Z. Xu, L. Chen, W. Gu, Y. Gao, L. Lin, Z. Zhang, Y. Xi, Y. Li, The performance of docetaxel-loaded solid lipid nanoparticles targeted to hepatocellular carcinoma, Biomaterials, 30 (2009) 226-232.
[42] J.-Z. Du, X.-J. Du, C.-Q. Mao, J. Wang, Tailor-made dual pH-sensitive polymer–doxorubicin

nanoparticles for efficient anticancer drug delivery, J. Am. Chem. Soc., 133 (2011) 17560-17563.
[43] C.C. Lee, E.R. Gillies, M.E. Fox, S.J. Guillaudeu, J.M.J. Fréchet, E.E. Dy, F.C. Szoka, A single dose of doxorubicin-functionalized bow-tie dendrimer cures mice bearing C-26 colon carcinomas, Proc. Natl. Acad. Sci. U. S. A., 103 (2006) 16649-16654.
[44] R. Tong, J. Cheng, Ring-opening polymerization-mediated controlled formulation of polylactide−drug nanoparticles, J. Am. Chem. Soc., 131 (2009) 4744-4754.
[45] O.P. Varghese, W. Sun, J. Hilborn, D.A. Ossipov, In situ cross-linkable high molecular weight hyaluronan−bisphosphonate conjugate for localized delivery and cell-specific targeting: A hydrogel linked prodrug approach, J. Am. Chem. Soc., 131 (2009) 8781-8783.
[46] W. Zhou, X.-H. Dai, C.-M. Dong, Biodegradable and biomimetic poly(ε-caprolactone)/poly(lactobionamidoethyl methacrylate) biohybrids: Synthesis, lactose-installed nanoparticles and recognition properties, Macromol. Biosci., 8 (2008) 268-278.
[47] Y. Mai, Y. Zhou, D. Yan, Synthesis and size-controllable self-assembly of a novel amphiphilic hyperbranched multiarm copolyether, Macromolecules, 38 (2005) 8679-8686.
[48] A.J. Harnoy, I. Rosenbaum, E. Tirosh, Y. Ebenstein, R. Shaharabani, R. Beck, R.J. Amir, Enzyme-responsive amphiphilic PEG-dendron hybrids and their assembly into smart micellar nanocarriers, J. Am. Chem. Soc., 136 (2014) 7531-7534.
[49] C. Shi, D. Guo, K. Xiao, X. Wang, L. Wang, J. Luo, A drug-specific nanocarrier design for efficient anticancer therapy, Nat. Commun., 6 (2015).
[50] C.J. Newcomb, S. Sur, J.H. Ortony, O.-S. Lee, J.B. Matson, J. Boekhoven, J.M. Yu, G.C. Schatz, S.I. Stupp, Cell death versus cell survival instructed by supramolecular cohesion of nanostructures, Nat. Commun., 5 (2014).
[51] T.G.W. Edwardson, K.M.M. Carneiro, C.K. McLaughlin, C.J. Serpell, H.F. Sleiman, Site-specific positioning of dendritic alkyl chains on DNA cages enables their geometry-dependent self-assembly, Nat. Chem., 5 (2013) 868-875.
[52] D. Wang, C. Tu, Y. Su, C. Zhang, U. Greiser, X. Zhu, D. Yan, W. Wang, Supramolecularly engineered phospholipids constructed by nucleobase molecular recognition: upgraded generation of phospholipids for drug delivery, Chem. Sci., 6 (2015) 3775-3787.
[53] D. Schmaljohann, Thermo- and pH-responsive polymers in drug delivery, Adv. Drug Del. Rev., 58 (2006) 1655-1670.
[54] C.B. Thompson, Apoptosis in the pathogenesis and treatment of disease, Science, 267 (1995) 1456.
[55] J. Noh, B. Kwon, E. Han, M. Park, W. Yang, W. Cho, W. Yoo, G. Khang, D. Lee, Amplification of oxidative stress by a dual stimuli-responsive hybrid drug enhances cancer cell death, Nat. Commun., 6 (2015).
[56] K. Tang, Y. Zhang, H. Zhang, P. Xu, J. Liu, J. Ma, M. Lv, D. Li, F. Katirai, G.-X. Shen, G. Zhang, Z.-H. Feng, D. Ye, B. Huang, Delivery of chemotherapeutic drugs in tumour cell-derived microparticles, Nat. Commun., 3 (2012) 1282.
[57] R. Mo, T. Jiang, R. DiSanto, W. Tai, Z. Gu, ATP-triggered anticancer drug delivery, Nat. Commun.., 5 (2014).
[58] A. Das, D. Durrant, C. Mitchell, E. Mayton, N.N. Hoke, F.N. Salloum, M.A. Park, I. Qureshi, R. Lee, P. Dent, Sildenafil increases chemotherapeutic efficacy of doxorubicin in prostate cancer and ameliorates cardiac dysfunction, Proc. Natl. Acad. Sci. U. S. A., 107 (2010) 18202-18207.
[59] R.J. Stockert, A.G. Morell, I.H. Scheinberg, Mammalian hepatic lectin, Science, 186 (1974) 365-366.
[60] R. Kanasty, J.R. Dorkin, A. Vegas, D. Anderson, Delivery materials for siRNA therapeutics, Nat Mater., 12 (2013) 967-977.
[61] F. Gao, Q. Yuan, L. Gao, P. Cai, H. Zhu, R. Liu, Y. Wang, Y. Wei, G. Huang, J. Liang, Cytotoxicity and therapeutic effect of irinotecan combined with selenium nanoparticles, Biomaterials, 35 (2014) 8854-8866.